

# The dichotomy of the halo of the Milky Way

Daniela Carollo<sup>\*</sup> and Timothy C. Beers<sup>†</sup>

*<sup>\*</sup>Research School of Astronomy and Astrophysics, Mount Stromlo Observatory, The Australian National University Mount Stromlo Observatory, Cotter Road, Weston, ACT 2611, Australia & INAF, Osservatorio Astronomico di Torino, 10025, Pino Torinese, Italy*

*<sup>†</sup>Department of Physics and Astronomy, Center for the Study of Cosmic Evolution, Joint Institute for Nuclear Astrophysics, Michigan State University, E. Lansing, Michigan 48824, USA*

**Abstract.** We summarize evidence that the halo of the Milky Way comprises two different, and broadly overlapping, stellar components. The two structures exhibit different chemical compositions, spatial distributions, and kinematics. These results were obtained through an analysis of more than 20,000 calibration stars from the Sloan Digital Sky Survey (SDSS). The duality of the stellar halo directly impacts galaxy formation models, for the Milky Way and other large spirals.

**Keywords:** Astronomy, Astrophysics, Milky Way, Galactic Halo

**PACS:** 90.98.35.Ac, 98.35.Df, 98.35.Gi, 98.35.Ln

## INTRODUCTION

The structure of the halo of the Milky Way has recently been revised by the work of Carollo et al. (2007) [1]. Confirming previous speculations based on much smaller data sets, the halo is indeed clearly divisible in two overlapping stellar components – the inner halo and the outer halo. The first structure dominates at  $R < 10\text{--}15$  kpc, exhibits highly eccentric stellar orbits, is in slightly prograde rotation, and comprises stars with a peak metallicity around  $[\text{Fe}/\text{H}] \sim -1.6$ . The outer halo is dominant at  $R > 15\text{--}20$  kpc, exhibits a much more uniform distribution in eccentricity, includes stars on highly retrograde orbits, and possesses a peak metallicity three times lower, i.e.  $[\text{Fe}/\text{H}] \sim -2.2$ . Previous work provided hints that the halo of the Milky Way may not comprise a single population, primarily based on analysis of the spatial profiles (or inferred spatial profiles) for halo objects, and possible indications of a net retrograde motion. In any case, the past samples of tracer objects were not sufficiently large to establish the dichotomy of the halo with confidence, and usually were suitable only for consideration of a limited number of the expected signatures of its presence. In Carollo et al. (2007) [1] all of the expected signals for the presence of two different stellar halo populations (different spatial distributions, kinematics, and chemical compositions) are now seen. This was made possible through the analysis of a homogeneously selected sample of more than 20,000 stars, originally obtained as calibration data during the course of the Sloan Digital Sky Survey (SDSS, [2]).

## DERIVATION OF THE KINEMATIC AND ORBITAL PARAMETERS

The total number of unique stars in the sample is 20,366, and comprises mainly F and G main-sequence turnoff stars. The apparent magnitude range is  $15.5 < g_0 < 17.0$  (spectrophotometric calibration stars), and  $17.0 < g_0 < 18.5$  (telluric calibration stars). The color ranges are  $0.6 < (u-g)_0 < 1.2$  ;  $0 < (g-r)_0 < 0.6$  (see Figure 1).

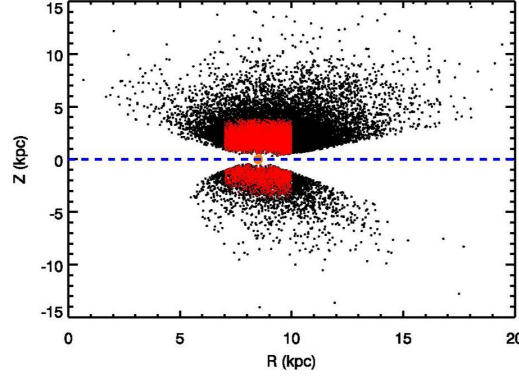


**FIGURE 1.** The spatial distribution of the SDSS-DR5 calibration stars in the Z-R plane, where Z is the distance from the Galactic plane, and R is the distance from the center of the Galaxy projected onto the Galactic plane. The dashed blue line represents the Galactic plane, while the filled orange dot is the position of the Sun, at  $Z = 0$  kpc and  $R = 8.5$  kpc. The “wedge shape” of the selection area is the result of limits of the SDSS footprint in Galactic latitude. The red points indicate the 11,458 stars that satisfy our criteria for a “local sample” of stars, having  $7 \text{ kpc} < R < 10 \text{ kpc}$ , with distance estimates from the Sun  $< 4$  kpc, and with viable measurements of stellar parameters and proper motions.

In order to derive the full space motions of the stars, we require astrometry (positions and proper motions), radial velocities, and distances. The SDSS provides positions with an accuracy of  $0.1''$ , while proper motions are provided by the re-calibrated USNO-B2 catalogue ([3]), with an accuracy of 3-4 mas/yr. The radial velocities are derived from matches to an external library of high-resolution spectral templates with accurately known velocities; its accuracy is around 5-20 km/s, depending on the S/N of the spectrum. The distances are evaluated using the cluster fiducials of Beers et al. (2000) [4]; the accuracy is around 10-20%. The SEGUE Stellar Parameter Pipeline (SSPP, [5, 6, 7]) provides the stellar physical parameters, i.e. effective temperature, surface gravity, and metallicity, with accuracies of 100 K, 0.25 dex, and 0.20 dex, respectively.

In order to obtain the best available estimates of the kinematic and orbital parameters for the stars in our sample, we consider only those stars satisfying several cuts: (1) A selection in the effective temperature range  $5000 \text{ K} < T_{\text{eff}} < 6800 \text{ K}$ , over which the SSPP is expected to provide the highest accuracy, reducing the number of stars to 19,687, (2) A selection for stars in the sample with distances  $d < 4$  kpc from the Sun, in order to restrict the kinematical and orbital analyses to a local volume (where the assumptions going into their calculation are best satisfied), reducing the number of stars to 15,435. The choice of stars in a local volume reduces errors in the derived transverse velocities, which scale with distance from the Sun. The number of stars in the remaining sample is 11,458. The proper motions, used in combination with radial velocities and the

estimated distances, provide the information required to calculate the full space motions ( $U, V, W$ ) of the stars relative to the Local Standard of Rest (LSR). We have also obtained the velocity components of the stars in a cylindrical reference frame with origin at the Galactic center ( $V_R, V_\Phi, V_Z$ ).

The orbital parameters are derived adopting a Stäckel-type gravitational potential that comprises a flattened oblate disk and a spherical massive dark halo ([8, 9]). The quantities obtained are  $r_{peri}$ , which correspond to the closest approach of an orbit to the Galactic center, and  $r_{apo}$ , which is the farthest extent of an orbit from the Galactic center. The orbital eccentricities and the maximum distance of stellar orbits above or below the Galactic plane,  $Z_{max}$ , are also evaluated.

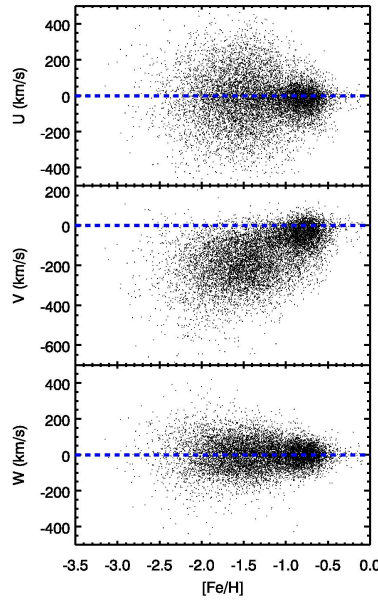


**FIGURE 2.** The  $U$ ,  $V$ , and  $W$  components of the space motions of stars in our sample as a function of  $[\text{Fe}/\text{H}]$ . A blue dashed line at 0 km/s has been added in each panel for reference. In the metallicity range  $-1.2 < [\text{Fe}/\text{H}] < -0.3$ , all three panels exhibit a low-velocity dispersion population of stars with mean values of the velocity components near 0 km/s, and dispersion in velocities of around 40-50 km/s. These are the stars of the thick-disk and metal-weak thick-disk populations. At metallicities below  $[\text{Fe}/\text{H}] \sim -1.2$ , the large velocity dispersions (on the order of 100 to 150 km/s) observed in each component are associated with the broadly overlapping inner- and outer-halo populations of stars.

## EVIDENCE FOR THE DICHOTOMY OF THE GALACTIC HALO

There exist multiple signatures for the dichotomy of the Galactic halo; space precludes a discussion of all of them (see [1]). The change in the distribution of stellar metallicity with the rotational velocity,  $V$  or  $V_\Phi$ , and  $Z_{max}$  is one of the stronger pieces of evidence. Figure 3 shows the Metallicity Distribution Function (MDF), for different values of  $Z_{max}$ , for stars with retrograde orbits. Stars from the disk population, which possess highly prograde orbits, cannot be present in this plot. We performed a Kolmogorov-

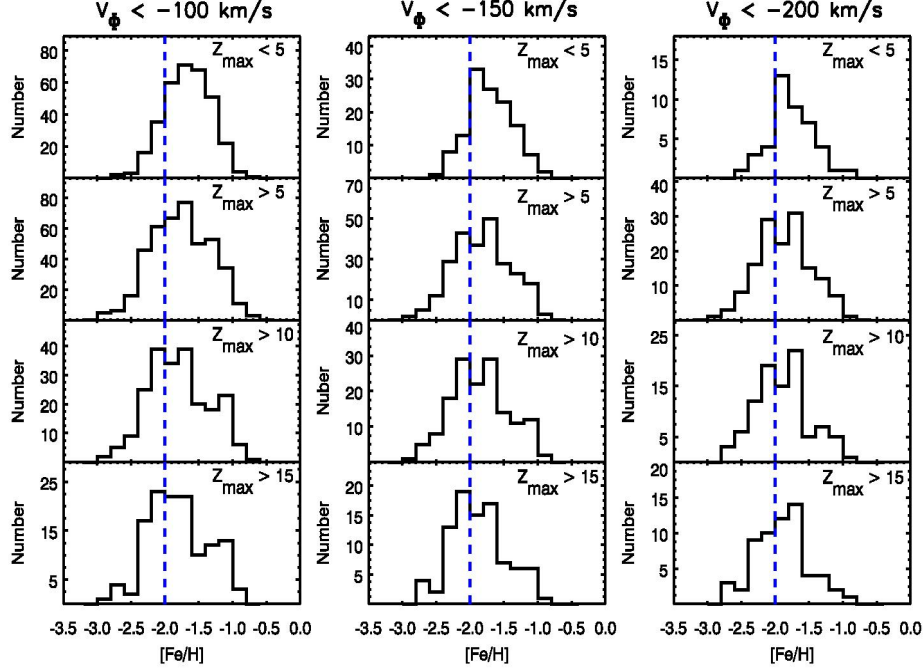


**FIGURE 3.** The distribution of  $[\text{Fe}/\text{H}]$  for the stars in our sample on highly retrograde orbits. The panels show various cuts in  $V_\phi$ , and for different ranges of  $Z_{\text{max}}$ . A blue dashed line at  $[\text{Fe}/\text{H}] = -2.0$  is added for reference. The left-hand column applies for stars with  $V_\phi < -100$  km/s; the clearly skewed distribution of  $[\text{Fe}/\text{H}]$  exhibits an increased contribution from lower metallicity stars as one progresses from the low ( $Z_{\text{max}} < 5$  kpc) to the high ( $Z_{\text{max}} > 15$  kpc) subsamples. Simultaneously, the predominance of stars from the inner-halo population, with peak metallicity at  $[\text{Fe}/\text{H}] \sim -1.6$ , decreases in relative strength, and shifts to lower  $[\text{Fe}/\text{H}]$ . Similar behaviors are seen in the middle and right-hand columns, which correspond to cuts on  $V_\phi < -150$  km/s and  $-200$  km/s, respectively.

Smirnov test of the null hypothesis that the MDFs of stars shown in the lower panels for the individual cuts on  $V_\phi$  could be drawn from the MDFs of the same parent population as those shown in the upper panels; the null hypothesis is strongly rejected at a high level of statistical significance. We thus conclude that the halo comprises stars with intrinsically different distributions in metallicity. This behavior, as well as an imbalance of the energy distributions for these stars (see [1] for details), would not be expected if “the halo” is a single entity. The local sample of SDSS calibration stars exhibits a (highly statistically significant) net retrograde rotation for the outer-halo component of  $V_\phi \sim -70$  km/s. This value is in agreement with the Frenk & White analysis ([10]), in which the rotational velocity is estimated on the basis of the radial velocity and the distance alone, so that there is no propagation of errors on the proper motions into the

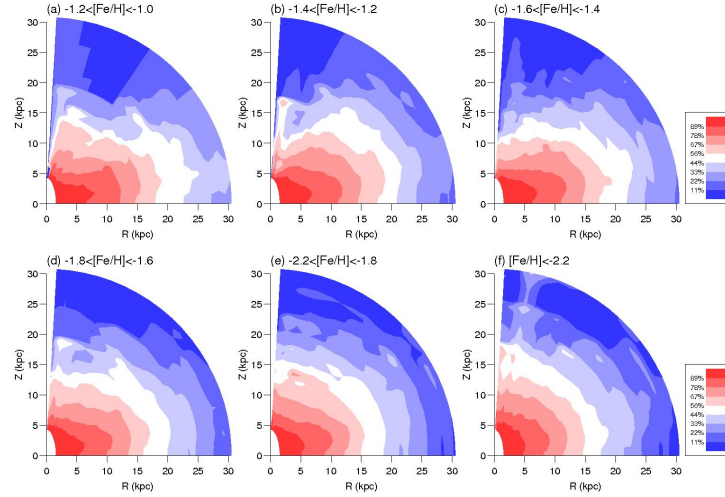


**FIGURE 4.** Equidensity contours of the reconstructed global density distributions for stars in our sample with various metallicities. The global density distributions are constructed from the sum of the probability density of an orbit at each location in this plane, with a weighting factor being inversely proportional to the corresponding density at the currently observed position of the star.

calculation of the kinematical quantities.

Other evidence for the duality of the Galactic halo can be obtained from an inversion of the orbital properties of the sample to obtain relative densities of the tracer population as a function of distance. Inspection of Figure 4 reveals that the inner regions are rather flattened at higher  $[\text{Fe}/\text{H}]$ . In particular, for the metallicity bin  $-1.4 < [\text{Fe}/\text{H}] < -1.8$  (third and fourth panel), the axis ratio is around 0.6. As  $[\text{Fe}/\text{H}]$  sweeps toward lower values, the spatial distribution becomes less flattened, and then roughly spherical at  $[\text{Fe}/\text{H}] < -2.2$  (axis ratio  $\sim 0.9$ ). This indicates that the inner-halo population dominates locally for stars with  $[\text{Fe}/\text{H}] > -2$ , whereas the outer-halo population dominates for all  $[\text{Fe}/\text{H}]$  at distances  $R > 15\text{--}20$  kpc, and also locally for stars with  $[\text{Fe}/\text{H}] < -2$ . Carollo et al. (2007) show that the inner and outer halos also exhibit different orbital characteristics as a function of metallicity.

## IMPLICATIONS OF THE DICHOTOMY OF THE HALO

The global properties of the outer-halo population clearly indicates that its formation is distinct from both the inner-halo population and the disk components of the Milky Way. Within the context of the  $\Lambda\text{CDM}$  paradigm, a possible scenario of the formation of the outer halo is the dissipationless chaotic merging of smaller subsystems within a pre-existing dark-matter-dominated halo. These subsystems were subjected to tidal disruption in the outer part of the dark-matter halo due to their lower masses ([11]). As candidate (surviving) counterparts for such subsystems, one might consider the currently

observed low-luminosity dwarf spheroidal galaxies surrounding the Galaxy, in particular the most extreme cases recently identified from the SDSS ([12, 13]).

The difference in the MDF of the inner/outer halo components has the important consequence that the lowest metallicity stars may be associated with the outer halo. This information could be used to search for the most metal-poor stars in future surveys, by selection of stars with highly retrograde proper motions. Other important issues related to the chemical difference of the two halo components should also be explored, e.g., the determination of the primordial lithium abundance from observations of the most metal-poor stars ([14]), and the existence of a possible relationship between the numbers of carbon-enhanced metal-poor stars as a function of declining metallicity ([15]), and as a function of distance from the Galactic plane ([16]).

Very recently, Koch et al. (2007) [17] reported the existence of a strong gradient in the abundance distribution of stars located along M31's minor axis, and towards their outer halo fields, which exhibit a metallicity  $[\text{Fe}/\text{H}] < -2$ . This finding is consistent with the present results found for the Milky Way. Although they may differ in detail, it appears that the two dominant galaxies of the Local Group have undergone similar accretion histories.

## ACKNOWLEDGMENTS

The authors are grateful to the organizers for providing assistance with travel and accomodation expenses. This work also received support from grants AST 07-07776 and PHY 02-15783; Physics Frontier Center / Joint Institute for Nuclear Astrophysics (JINA), awarded by the US National Science Foundation.

## REFERENCES

1. D. Carollo et al., *Nature*, **450**, 1020–1025 (2007).
2. D. G. York et al., *Astron. J.*, **120**, 1579–1587 (2000).
3. J. A. Munn et al., *Astron. J.*, **127**, 3034–3042 (2004).
4. T. C. Beers et al., *Astron. J.*, **119**, 2866–2881 (2000).
5. Y. S. Lee et al. (a), *Astron. J.*, submitted, arXiv: 0710.5645 (2008a).
6. Y. S. Lee et al. (b), *Astrophys. J.*, submitted, arXiv: 0710.5778 (2008b).
7. C. Allende Prieto et al., *Astrophys. J.*, submitted, arXiv:0711.2886 (2008).
8. T. de Zeeuw, *Mon. Not. R. Astr. Soc.*, **216**, 599–612 (1985).
9. H. Dejonghe & T. de Zeeuw, *Astrophys. J.*, **333**, 90–129 (1988).
10. C. S. Frenk & S. D. M. White, *Mon. Not. R. Astr. Soc.*, **193**, 295–311 (1980).
11. K. Bekki & M. Chiba, *Astrophys. J.*, **558**, 666–686 (2001).
12. V. Belokurov et al., *Astrophys. J.*, **642**, L137–L140 (2006).
13. V. Belokurov et al., *Astrophys. J.*, **654**, 897–906 (2007).
14. P. Bonifacio et al., *Astrophys. J.*, **462**, 851–864 (2007).
15. S. Lucatello et al., *Astrophys. J.*, **653**, L37–L40 (2006).
16. J. Tumlinson, *Astrophys. J.*, **665**, 1361–1370 (2007).
17. A. Koch et al., *Astrophys. J.*, submitted, arXiv: 0711.4588 (2007).